Ab initio line-shape calculations for the S and O branches of H2 perturbed by He

H. Jóźwiak, Franck Thibault, N. Stolarczyk, P. Wcislo

Ab initio line-shape calculations for the S and O branches of H_2 perturbed by He

Hubert Jóźwiak, Franck Thibault, Nikodem Stolarczyk, Piotr Wcisło

PII: S0022-4073(18)30428-X
DOI: https://doi.org/10.1016/j.jqsrt.2018.08.023
Reference: JQSRT 6195

To appear in: *Journal of Quantitative Spectroscopy & Radiative Transfer*

Received date: 8 June 2018
Revised date: 24 August 2018
Accepted date: 24 August 2018

Please cite this article as: Hubert Jóźwiak, Franck Thibault, Nikodem Stolarczyk, Piotr Wcisło, Ab initio line-shape calculations for the S and O branches of H_2 perturbed by He, *Journal of Quantitative Spectroscopy & Radiative Transfer* (2018), doi: https://doi.org/10.1016/j.jqsrt.2018.08.023

Highlights

- Close-coupling calculations of pressure broadening and shifting coefficients
- Close-coupling calculations of Dicke parameters
- Data for anisotropic Raman S (j=0-5) and O (j=2-5) lines for purely rotational transitions, fundamental band and first four overtones

Ab initio line-shape calculations for the S and O branches of H_2 perturbed by He

Hubert Jóźwiak[1*], Franck Thibault[2], Nikodem Stolarczyk[1] and Piotr Wcisło[1]

[1] *Institute of Physics, Faculty of Physics, Astronomy and Informatics, Nicolaus Copernicus University, Grudziadzka 5, 87-100 Toruń, Poland*

[2] *Institut de Physique de Rennes, UMR CNRS 6251, Université de Rennes 1, Campus de Beaulieu, Bât.11B, F-35042 Rennes, France*

Abstract

We report the results of *ab initio* investigation of the S and O branches of the hydrogen molecule perturbed by helium atom. The calculations, based on close-coupling scheme, were performed for vibrational bands from v=0 to v=5, and rotational levels up to j=5. We provide the pressure broadening and shifting coefficients and the real and imaginary parts of Dicke contribution to the Hess profile. The results are important for astrophysical studies, for example as a reference data for studying the gas giants' atmospheres.

Keywords: H_2, hydrogen, He, helium, line-shape parameters, molecular collisions, quantum scattering

1. Introduction

Hydrogen molecule is the most abundant molecule in the universe. Its importance in astrophysical studies has been thoroughly reviewed in Ref. [1]. Let us remind that the accurate values of pressure broadening and shifting coefficients are needed for the spectroscopic studies of the gas giants' atmospheres [2, 3]. Moreover, the simplicity of the H_2-He system allows highly accurate *ab initio* potential energy surface to be calculated and verified experimentally.

Email address: hubert.jozwiak@stud.umk.pl (Hubert Jóźwiak[1*])

*Corresponding author

The goal of this paper is to provide the fully *ab initio* line-shape parameters for H_2 in helium baths. In a recent paper [4], some of the present authors reported a new potential energy surface for this system and provided line-shape parameters for Raman isotropic and anisotropic Q lines. The latter parameters can be also used for electric quadrupole Q lines. In addition, this PES [4] was recently successfully tested on the very first purely rotational Stokes lines of D_2 in He [5]. Here, we investigated the anisotropic Raman S and O lines of H_2 in He, for vibrational bands from 0-0 up to 0-5, for rotational levels from j=0 to j=5 for S lines, and from j=2 to j=5 for O lines. We report the pressure broadening and shifting coefficients and both real and imaginary part of the Dicke parameter. We have calculated them by averaging the generalized spectroscopic cross sections for 18 temperatures, ranging from 5 to 2000 K. The generalized spectroscopic cross sections were calculated using S-matrix elements provided by the MOLSCAT [6] code.

2. Quantum scattering calculations

In this section we report the details of *ab initio* quantum scattering calculations for the H_2-He system. The potential energy surface (PES) in the examined system depends on the distance between the hydrogen molecule and the helium atom, R, the intramolecular distance, r_{HH}, and the angle between these two axis, θ. We made use of the PES which was recently reported in Ref. [4], which is an extension of the Bakr et al. PES [7]. It has recently been shown [1] that the PES from Ref. [7] is more accurate than the previous PESs ([8, 9, 10]). However, it was pointed out, that the PES from Ref. [7] does not cover large enough vibration amplitude in H_2 and therefore should not be used to study the overtones. Not only does the most recent PES [4] cover the sufficient range of the interatomic distance, r_{HH}, but it also properly describes the asymptotic behavior of the interaction energy in this system. For more details see [4].

The PES is expanded over Legendre polynomials, P_λ:

$$V(R, r_{HH}, \theta) = \sum_\lambda V_\lambda(R, r_{HH}) P_\lambda(\cos(\theta)). \quad (1)$$

Since H_2 is a homonuclear molecule, the λ index takes only even values, and due to the small anisotropy of the PES, it is sufficient to retain only the first 4 terms of the expansion. The obtained terms $V_\lambda(R, r_{HH})$ are averaged over rovibrational wavefunctions of the H_2 molecule $\chi_{j,v}(r_{HH})$, which gives the radial coupling terms $V_{\lambda,v,j,v',j'}(R)$. For transitions between different vibrational states, one can neglect the centrifugal distortion [1], and write the radial coupling terms as $V_{\lambda,v,0,v',0}(R)$. Thus for rovibrational transitions we consider 2*4 radial coupling terms. While considering purely rotational transitions, one should take into consideration the centrifugal distortion. This phenomenon was firstly studied by Shafer and Gordon [11], and latter by Dubernet and Tuckey [12], who have shown that it has a relatively small effect effect for the broadening but a rather large one for the shift. This is due to the fact, that the line shift is very sensitive to the difference in the elastic scattering in the two different rotational states. Therefore, in this case, one cannot average the terms $V_\lambda(R, r_{HH})$ over rovibrational wavefunctions with j set to 0. In order to obtain proper results, we have prepared the radial coupling terms $V_{\lambda,0,j,0,j'}(R)$ with j up to 15 and 14, for ortho and para states, respectively. Thus for purely rotational transitions we have to consider 144 radial coupling terms.

We performed close-coupling calculations for this system using the MOLSCAT [6] code, obtaining the S-matrix elements. We used them to calculate the generalized spectroscopic cross section [13, 14]:

$$\sigma_\lambda^q(v_i, j_i, v_f, j_f, E_{kin}) =$$
$$\frac{\pi}{k^2} \sum_{J_i, J_f, l, l', \bar{l}, \bar{l}'} (-1)^{l-l'-\bar{l}+\bar{l}'} [J_i][J_f]$$
$$\times \sqrt{[l][l'][\bar{l}][\bar{l}']} \begin{pmatrix} l & \bar{l} & \lambda \\ 0 & 0 & 0 \end{pmatrix} \begin{pmatrix} l' & \bar{l}' & \lambda \\ 0 & 0 & 0 \end{pmatrix} \begin{bmatrix} j_i & j_i & \bar{l} & \bar{l}' \\ j_f & l & j_f & l' \\ q & J_f & J_i & \lambda \end{bmatrix}$$
$$\times i^{l-l'-\bar{l}+\bar{l}'} [\delta_{ll'}\delta_{\bar{l}\bar{l}'} - \langle v_i j_i l' | S^{J_i}(E_{T_i}) | v_i j_i l \rangle \langle v_f j_f \bar{l}' | S^{J_f}(E_{T_f}) | v_f j_f \bar{l} \rangle^*]. \quad (2)$$

The rovibrational transition is denoted as $v_i, j_i \rightarrow v_f, j_f$, where i and f are the indexes of the initial and final states, respectively. J is the total angular

momentum, l is the relative kinetic momentum, and $\mathbf{J} = \mathbf{j}+\mathbf{l}$. k is the wavevector associated with the initial kinetic energy. $[x]$ denotes $(2x+1)$, quantities in parentheses are Wigner 3j and the quantity in bracket is a Wigner 12j symbol of the second kind [15]. The total energies associated with each of the rovibrational energy levels are denoted as $E_{T_i} = E_{kin} + E_{v_i j_i}$ and $E_{T_f} = E_{kin} + E_{v_f j_f}$. The tensor order of the radiation-matter interaction is denoted as q, and for the investigated here anisotropic (or equivalently absorption quadrupole) S and O lines, q=2. Equation (2) is a quite complex formula which involves a number of angular momenta and S-matrix elements. The summation over the six angular momenta reduces to a summation over only four of them for the case of λ=0. Moreover, in this case, the total angular momenta are in a triangular relation with q, and the Wigner 12j symbol can be transformed into a product of two Wigner 6j symbols. Thus, for λ=0, Eq.(2) reduces to the standard generalized spectroscopic cross section σ_0^q [1, 11, 16, 17], whose real and imaginary parts are referred to as the pressure broadening (PBXS) and pressure shifting (PSXS) cross sections, respectively. For λ=1, Eq.(2) transforms into the complex Dicke cross section (DXS) σ_1^q [5, 13, 14, 18]. Considering the vector nature of the velocity (a rank-1 tensor), the velocity-changing collisions induce additional angular momenta coupling. The summation is still over six angular momenta and there is no simple triangular rule for J_i, q and J_f. Thus, Dicke cross sections are more averaged quantities than PBXS and PSXS.

We took advantage of the fact, that the PES does not couple ortho and para states of H_2. While constructing the basis for the calculations, we dealt with even and odd rotational levels separately. The calculations of the cross sections were performed for 263 kinetic energies, ranging from 0.1 to 9000 cm^{-1}. The basis included rotational levels up to j=15 and j=14 for ortho and para states of H_2 molecule, respectively. One asymptotically closed level was retained in the calculations, apart from the kinetic energies larger than 7000 cm^{-1}. The energy levels of the rovibrational states were taken from Komasa et al. [19].

3. Line-shape parameters and collisional integrals

In this section we use generalized spectroscopic cross section to calculate the spectral line-shape parameters: pressure broadening and shifting coefficients, Γ_0 and Δ_0, as well as the real and imaginary part of the Dicke coefficient (which is also referred to as the frequency of optical velocity-changing collisions), ν^r_{opt} and ν^i_{opt}, respectively.

The first step is to calculate *ab initio* collision integrals $\omega^{s,s'}_{\lambda}$:

$$\omega^{s,s'}_{\lambda}(q) = \langle v \rangle \int dx x^{(s+s'+2)/2} e^{-x} \sigma^q_{\lambda}(v_i j_i v_f j_f; E_{kin} = x k_b T), \tag{3}$$

where $\langle v \rangle = \sqrt{8 k_b T / \pi \mu}$ is the mean relative speed of the particles. The spectroscopic line-shape parameters are related to the collision integrals in the following way [4]:

$$\gamma_0 = Re\left(n_b \omega^{00}_0(q)\right)\kappa, \tag{4}$$

$$\delta_0 = -Im\left(n_b \omega^{00}_0(q)\right)\kappa, \tag{5}$$

$$\tilde{\nu}^r_{opt} = Re\left(n_b m_b \frac{\frac{2}{3}\omega^{11}_1(q) - \omega^{00}_0(q)}{m_a + m_b}\right)\kappa, \tag{6}$$

$$\tilde{\nu}^i_{opt} = -Im\left(n_b m_b \frac{\frac{2}{3}\omega^{11}_1(q) - \omega^{00}_0(q)}{m_a + m_b}\right)\kappa, \tag{7}$$

where m_a and m_b are the masses of the active molecule and perturber atom respectively, and n_b is the number density of the bath. Those parameters are rescaled with κ coefficient, which stands for the definition of units, such that these are in the units of $\mathrm{cm}^{-1}/\mathrm{atm}$, with

$$\kappa = \frac{1}{2\pi c} \times \left(\frac{T_0}{p_0 T}\right), \tag{8}$$

where $T_0 = 273.15$ K and $p_0 = 1$ atm$= 101.325$ kPa.

The final line-shape parameters can be obtained in the following way: $\Gamma_0 = \gamma_0 p$, $\Delta_0 = \delta_0 p$, $\nu^r_{opt} = \tilde{\nu}^r_{opt} p$, $\nu^i_{opt} = \tilde{\nu}^i_{opt} p$, where p is the helium pressure.

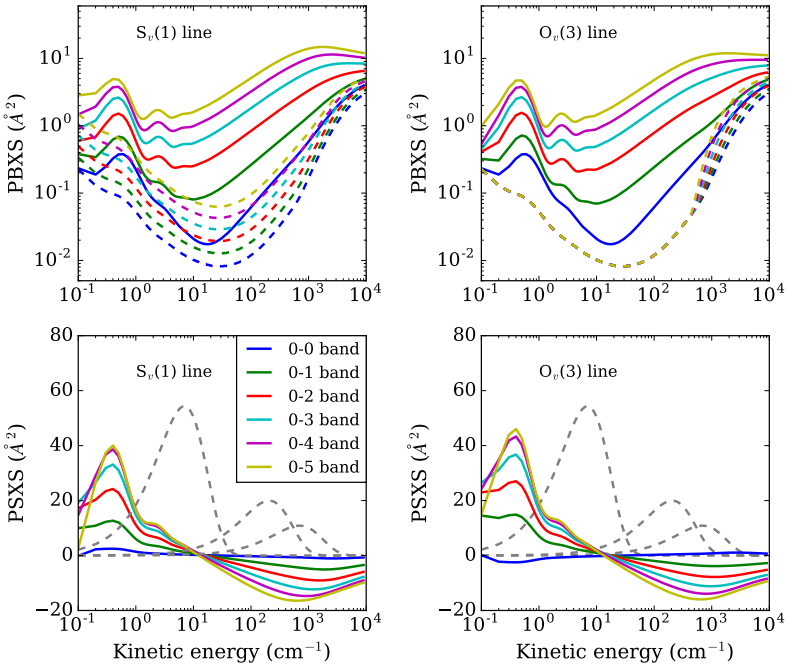

Figure 1: Comparison of pressure broadening and shifting cross sections between $S_v(1)$ and $O_v(3)$ lines in various vibrational bands at different kinetic energies (solid lines). The index v denotes the final vibrational quantum number. The inelastic contributions to the PBXS are presented in the upper panels (dashed lines). The Maxwell-Boltzmann distributions at 10, 296 and 1000 K are represented as dashed gray lines in the lower panels.

4. Results

In this section we report the results of our calculations of the pressure broadening, shifting cross sections along with the Dicke cross sections, as well as the obtained line-shape parameters. Our calculations produced a large quantity of data, and we only present some representative examples here. The full set of results can be found in the supplementary materials [20].

4.1. Generalized spectroscopic cross-sections

The goal of the following discussion is to give a brief look into the rotational and vibrational dependences of the cross sections, as well as the similarities

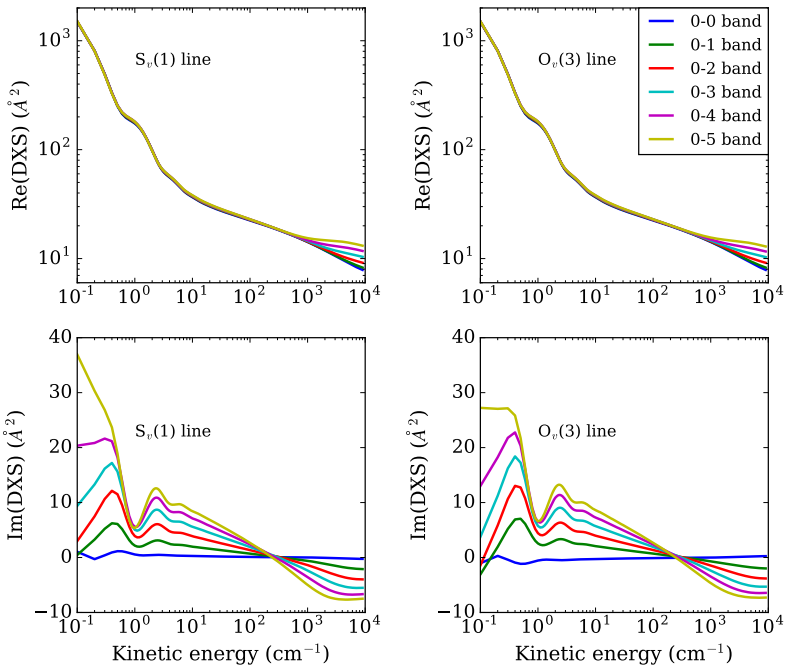

Figure 2: Comparison of real and imaginary parts of Dicke cross sections between $S_v(1)$ and $O_v(3)$ lines in various vibrational bands at different kinetic energies. The index v denotes the final vibrational quantum number.

between S and O lines. In general, the calculated cross sections have a similar behavior. We chose $S_v(1)$ and $O_v(3)$ lines to provide a graphical comparison of the cross section between different vibrational bands (Figs. 1,2), and the fundamental band to give an example of the dependency of the cross sections on the rotational number j (Figs. 3,4). The rest of the data can be found in the supplementary materials for this paper [20].

Figure 1 shows the pressure broadening and shifting cross sections as a function of the kinetic energy for various vibrational bands for the $S_v(1)$ and $O_v(3)$ lines, as well as the contributions to the broadening from the inelastic cross sections (see Eqs. (A.2) and (A.3) in Ref. [1]). Overall, it can be seen, that the behavior of the cross sections for S and O lines is quite similar. First, let us

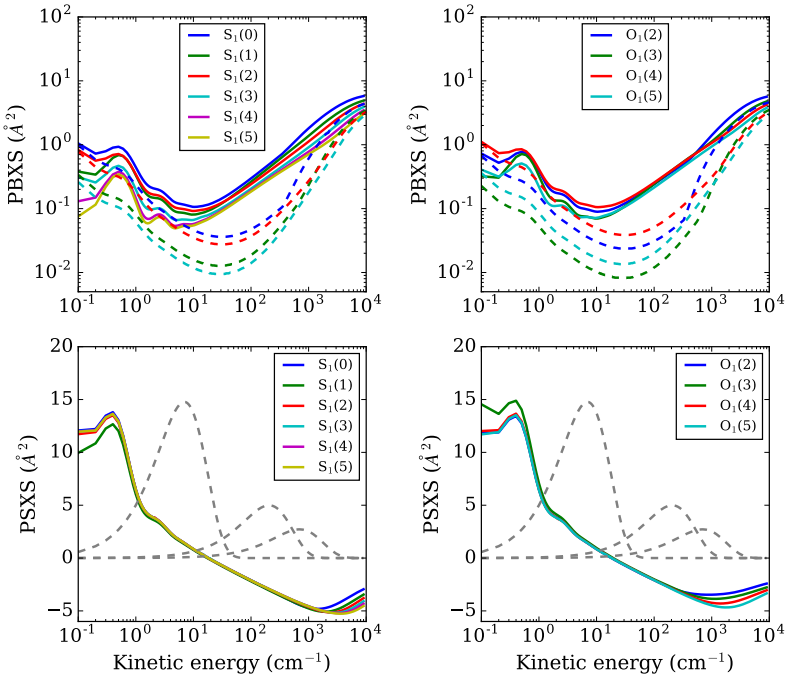

Figure 3: Comparison of pressure broadening and shifting cross sections between S and O lines in the fundamental band at various kinetic energies. The inelastic contributions to the PBXS for the S_1(0-3) and O_1(2-5) lines are presented in the upper panels (dashed lines). The Maxwell-Boltzmann distributions at 10, 296 and 1000 K are represented as dashed gray lines in the lower right panel.

consider the purely rotational $S_0(1)$ and $O_0(3)$ lines. As expected, the pressure broadening cross sections are identical, while the pressure shifting cross sections have opposite sign. This phenomenon was observed for all investigated purely rotational lines during this investigation, and was previously noticed in earlier studies [5, 16]. The values of the PBXS and PSXS are small, comparing to the other vibrational bands, due to the fact, that there is no vibrational phase shift. Moreover, the dephasing between j=1 and j=3 may be small. For kinetic energies in range from 0.1 cm^{-1} to 10 – 20 cm^{-1}, values of the PBXS decrease, before growing up. At the minimum, a change of the sign of the PSXS is observed. A tentative explanation is the following: the very low kinetic energies

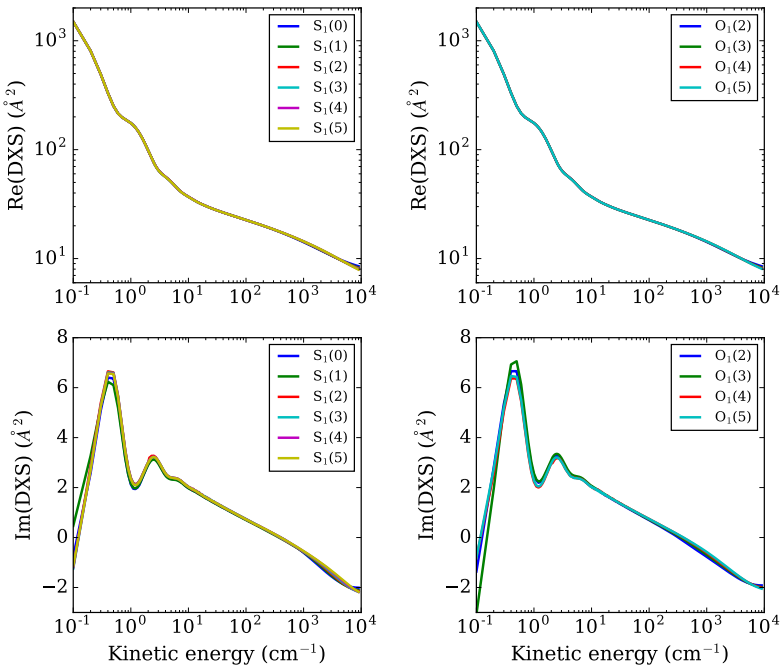

Figure 4: Comparison of real and imaginary part of Dicke cross sections between S and O lines in the fundamental band at various kinetic energies.

sample the long range attractive part of the potential, and as the kinetic energy increases, the repulsive part of the potential plays a more important role (recall that the overall PES well depth is about 10 cm^{-1}). Thus, it is possible that the shift, which result from the difference of scattering phase shifts (see Eq. (A.4) in Ref. [1]), may change its sign while passing from the very low kinetic energies to higher ones. Note also, that analogously to vibrational transitions (see below) the difference $V_{0,0,j_i,0,j_i}(R) - V_{0,j_f,0,j_f}(R)$ changes its sign while passing from the long to the short range part of the potential. As the kinetic energy increases, the role of the inelastic collisions increases and the values of the PBXS increase (see the inelastic cross sections in the Fig. 1). Ultimately, the purely rotational phase shift should tend to 0.

A similar discussion has already been reported around Figs. 13 and 14 of

Ref. [1] for the pressure broadening and shifting cross sections of the $S_0(1)$ line. In addition, the role of the isotropic components of the PES was discussed for both cross sections.

Let us now consider rovibrational transitions. In these cases, at least at low kinetic energies, a large contribution to the pressure broadening and shifting cross sections comes from the vibrational dephasing, which arises from the difference in the isotropic components of the PES in $v = 0$ and in v (see Fig. 4 of Ref. [4]): $\Delta V_0(R) = V_{0,0,0}(R) - V_{0,v,v}(R)$. This difference increases for 0-v transitions with v. Since this difference varies with R, its contribution to the pressure broadening and sifting cross sections varies with the kinetic energy. Moreover, as the kinetic energy increases, the contribution from the inelastic cross section increases. The inelastic cross sections increase with v because the spacing between the rotational energy levels in a given vibrational state decreases with v. One should also realize, that the inelastic contribution to the PBXS, presented in Fig. 1 is the same for $S_0(j)$ and $O_0(j+2)$ lines, while for rovibrational $S_v(j)$ and $O_v(j+2)$ lines this contribution is different. This is due to the slight differences between the radial terms of the potential in $v = 0$ and in v (as v increases, so does the interaction energy) and a strong variation of the energy spacing between the rotational levels with v. For example the difference between the rotational levels $E_{v=0}(j = 3) - E_{v=0}(j = 1)$ is about 587 cm^{-1}, while the difference between $E_{v=5}(j = 3) - E_{v=5}(j = 1)$ is about 444 cm^{-1}. These considerations explain why the absolute values of the pressure broadening and shifting cross sections increase with v. As the energy increases (above about 600 cm^{-1}) the inelastic cross sections increase abruptly, and the magnitude of the PSXS decreases. Finally, a sign change of the PSXS is observed around 20 cm^{-1}, that may come from a sign change of the difference between the isotropic parts of the PES in $v = 0$ and in v, $\Delta V_0(R)$. Such analysis was performed for isotropic and anisotropic $Q_v(2)$ lines in Figs. 5 and 7 of Ref. [4], in terms of the vibrational dephasing, full dephasing and inelastic contributions.

Figure 2 shows an analogous comparison but for the real and imaginary parts of Dicke cross sections (DXS). It can be seen, that the values of the

Re(DXS) are equal for the $S_0(1)$ and $O_0(3)$ lines, while their imaginary parts have opposite sign [5]. Similar to the $Q_v(2)$ lines, discussed in Ref. [4] (see Fig. 9 therein), the real part of the Dicke cross sections are nearly indistinguishable for kinetic energies lower than about 600 cm^{-1}. Above this value, the values of the Re(DXS) split for different vibrational transitions. This may be due to the greater influence of the inelastic transitions. The influence of the vibrational quantum number (and of the vibrational dephasing) is more clearly seen for the imaginary parts of the Dicke cross sections, whose absolute values increase with v. Similar to the PSXS, a sign change occurs, but for larger kinetic energies (beween 260 and 375 cm^{-1}), which should be related to the variation of the inelastic cross sections. Once again, such behavior is similar to the one noticed in Fig. 11 of Ref [4] for $Q_v(2)$ lines.

Fig. 3 presents the comparison of various S and O lines in the fundamental band in order to show the rotational dependence of the cross sections with j. Generally speaking, the PBXS for low j are sensitive to both the long and short range parts of the PES, while for high j values the PBXS are mostly sensitive only to the short range part. Thus, the PBXS are expected to decrease with increasing j. The inelastic contribution is also expected to be more important for low j values, because for a given vibrational state, the rotational energy spacing increases with j. However, this is not that simple[1], because of the ortho/para separation and because the inelastic contribution depends on the kinetic energy. If the kinetic energy is too small, a molecule in j=0 or in j=1 cannot relax or reach an excited level (see the increase of the inelastic contributions to the $S_1(0)$ and $O_1(2)$ pressure broadening cross sections around 350 cm^{-1}, associated with the opening of the $v = 0$, $j = 2$ and $v = 1$, $j = 2$ levels, respectively). Clearly, the contribution of the inelastic collisions increases for kinetic energies larger than a few hundreds of wavenumbers for all the lines

[1]See Table V of Ref. [21], which provides thermally averaged values of the cross sections at various temperatures for Q lines of the fundamental band and Fig. 13 of Ref. [4], which provides values for isotropic and anisotropic Raman Q lines at room temperature.

considered. The dephasing contribution to the PBXS (Eq. (A4) of [1]) must be considered too. If we assume that it does not depend on j (which is the case for a purely vibrational dephasing, coming from the differences of the isotropic parts of the PES in v=0 and in v=1), then its contribution would be the same for S_1(j) lines (or O_1(j) lines). This is roughly observed for kinetic energies larger than about 1000 cm^{-1}. At the lowest kinetic energies (except below 1 cm^{-1}) the main contribution to the PBXS comes from the dephasing contribution. Since it slightly depends on j [1, 4], this is mainly a vibrational contribution. Concerning the PSXS, the values for the O and S lines, all together, do not differ very much for a very wide range of kinetic energies[2] (between about 1 and 1000 cm^{-1}) because they mainly originate from the vibrational phase shift. In the highest energy domain, above 1000 cm^{-1}, we observe a splitting of the S_1(j) and O_1(j) shifts, due to the competition between the inelastic transitions and the elastic ones (see Fig. 11 of Ref. [1]).

Figure 4 shows the comparison between Dicke cross sections for different lines of the fundamental band. The real part of these XSs are almost identical for the whole examined kinetic energy range, and there is no clear j dependence. Similar situation occurs while discussing the imaginary part of these cross sections. The main differences between S and O lines can be observed for kinetic energies lower than 1 cm^{-1}.

The behavior of the cross sections for kinetic energies below 1 cm^{-1} is difficult to interpret. At first sight, these calculations are expected to be more simple. In fact, this is not the case because the wavelength of the scattered wavefunction strongly varies from infinity to the small R distance. Moreover, the results are very sensitive to the input parameters of the propagator. However, it can be seen from Figs. 1 and 2, where the probability density function of the Maxwell-Boltzmann distribution is presented, that the results below 1 cm^{-1} do not influence the final line-shape parameters for temperatures larger than

[2]See Table II of Ref. [21] for Q_1(j) lines and Fig. 14 of Ref. [4], which provide thermally averaged values of the cross sections at room temperature.

10 K.

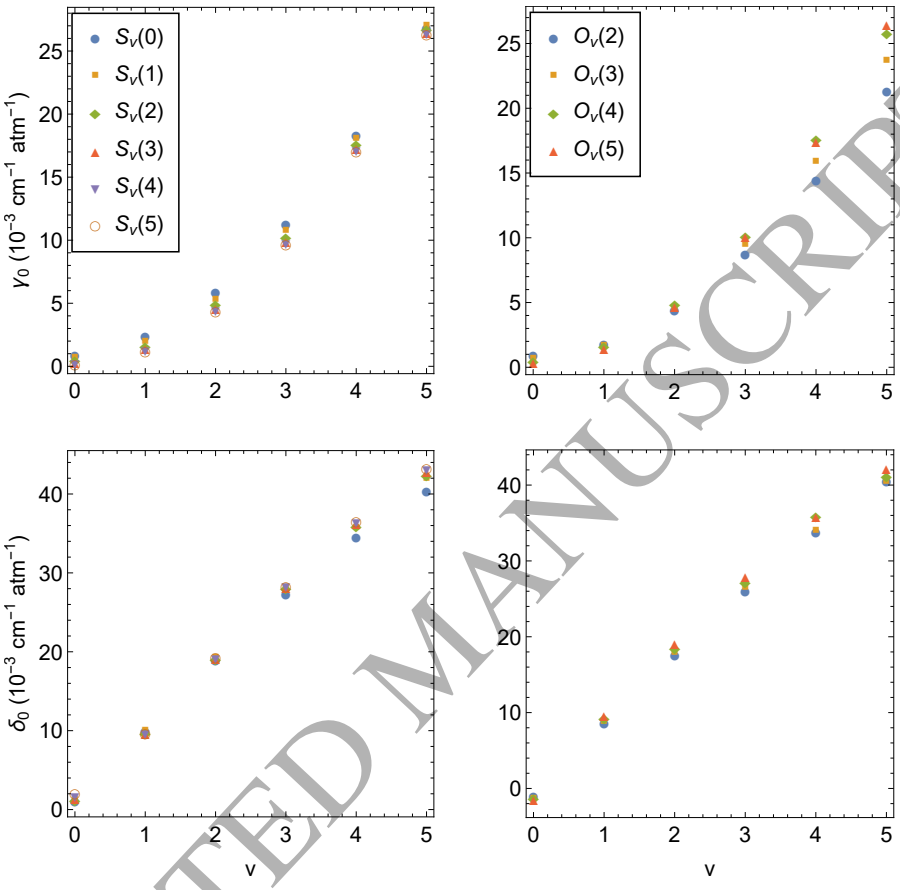

Figure 5: Comparison of pressure broadening, γ_0, and pressure shift, δ_0, coefficients at 296 K as a function of the final vibrational state for the $0 \rightarrow v$ bands.

4.2. Line-shape parameters

In this subsection we present the dependence of the line-shape parameters on the final vibrational number v of the transition. We chose to present in graphical form the results at the temperature of 296 K. The coefficients at different temperatures can be found in the supplementary materials [20]. The pressure broadening coefficients, shown in the Fig. 5, increase with v for both S

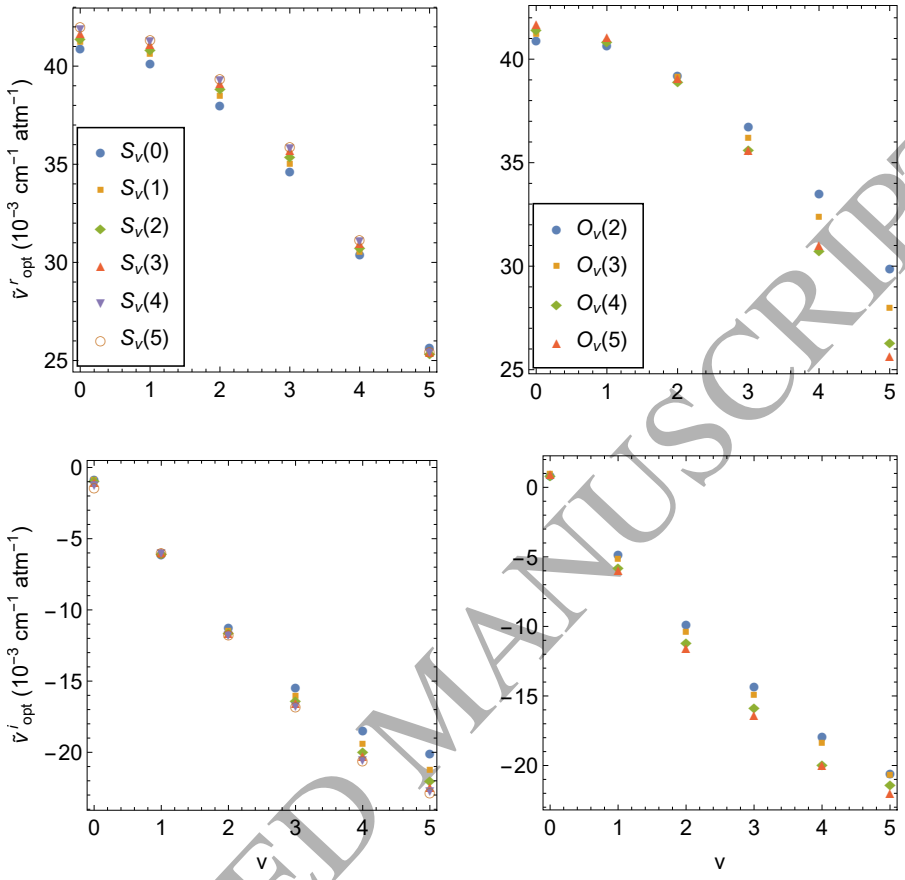

Figure 6: Comparison of real and imaginary parts of Dicke parameter, $\tilde{\nu}_{opt}$, at 296 K as a function of the final vibrational state for the $0 \rightarrow v$ bands.

and O lines. However, in case of O lines, the difference between the rotational numbers of the initial states, j, is more significant. We have no clear explanation for that. However, we note here, that the inelastic contribution to the pressure broadening cross sections for S(j) and O(j+2) lines are quite different. This could cause the difference in the dependence of γ_0 on j for the S and O lines. The pressure shift coefficients follow similar trend, increasing with v in case of both lines, as predicted. Figure 6 provides comparison for the real and imaginary parts of the Dicke parameter. The real part clearly depends on v, and for O

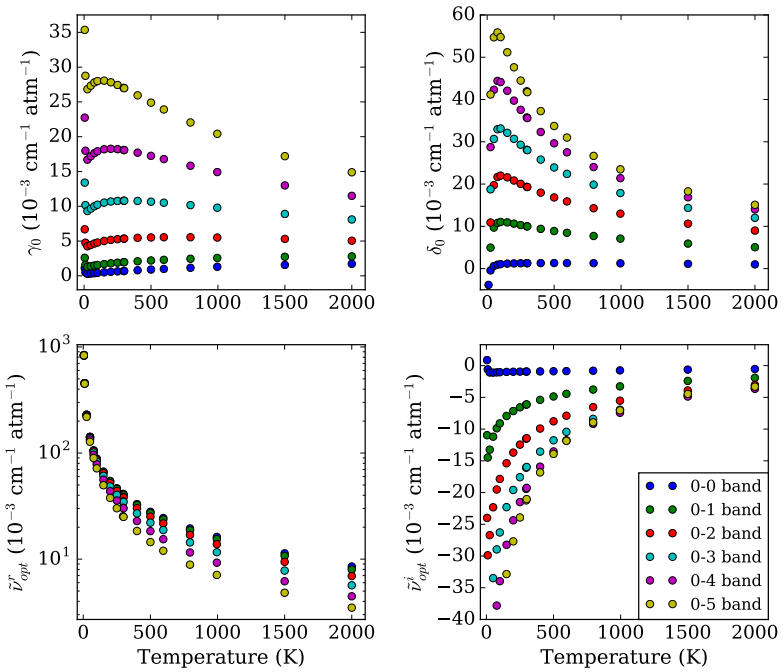

Figure 7: Pressure broadening, γ_0, and pressure shift, δ_0, coefficients, real and imaginary parts of the Dicke parameter, $\tilde{\nu}_{opt}$, for the $S_v(1)$ lines as a function of temperature.

lines, as the vibrational quantum number v increases, the dependence on the rotational quantum number is quite significant. For the imaginary part, the dependence on the vibrational quantum number is very similar for both S and O lines, with a quite small j dependence for a given vibrational band.

The line-shape parameters were calculated at 18 temperatures between 5 and 2000 K. Figure 7 presents the temperature dependence of all the four reported coefficients of the $S_v(1)$ line in various vibrational bands. The behavior of the pressure broadening and shift coefficients is similar to the one observed for Q lines [4]. The strong dependence on T and v can also be observed for the real and imaginary parts of the Dicke parameter, with a slight decrease of the absolute values of $\tilde{\nu}^i_{opt}$ for higher vibrational bands in temperatures above 500 K.

Table 1: Half width at half maximum (HWHM) for the $S_0(j)$ lines in 10^{-3} cm^{-1} amg^{-1}. Besides the typical Lorentzian contribution, γ_0, we present the effective half width at half maximum, $\gamma^\dagger$, taking into account all the line-shape effects (both the velocity-changing collisions and speed-dependent effects). The inhomogeneous component of the broadening due to the speed-dependence of the line shift (see Eq. (9)) is denoted as γ_δ. The values in parenthesis indicate the 1σ standard uncertainty.

j	Temperature (K)	γ_0	γ_δ	$\gamma^\dagger$	Experiment
0	45	0.067(1)	0.00027(1)	0.067(1)	0.11(1)[a]
	100	0.179(3)	0.00106(2)	0.179(3)	0.16(1)[a]
	150	0.321(5)	0.00253(4)	0.322(5)	0.34(2)[a]
	296	0.97(2)	0.0131(3)	0.98(2)	1.00(1)[b]
	311	1.06(2)	0.0146(3)	1.06(2)	1.12(4)[a]
	600	3.18(3)	0.052(2)	3.13(5)	3.07(15)[b]
	795	4.95(7)	0.075(2)	4.82(7)	4.76(26)[b]
	995	6.95(11)	0.092(2)	6.66(10)	6.29(33)[b]
1	26.7	0.027(1)	0.00045(2)	0.027(1)	0.09(1)[a]
	45	0.050(10)	0.00092(3)	0.051(10)	0.11(2)[a]
	100	0.153(3)	0.00282(5)	0.155(3)	0.16(1)[a]
	150	0.275(4)	0.0051(2)	0.279(4)	0.31(1)[a]
	296	0.75(1)	0.0149(3)	0.75(1)	0.78(3)[b]
	311	0.80(2)	0.0162(3)	0.81(2)	0.86(4)[a]
	600	2.18(4)	0.051(2)	2.19(4)	2.14(3)[b]
	795	3.36(5)	0.080(2)	3.34(5)	3.30(14)[b]
	995	4.72(7)	0.109(2)	4.65(7)	4.66(15)[b]
2	200	0.339(6)	0.0088(2)	0.344(5)	0.32(2)[a]
	292	0.57(1)	0.0150(3)	0.58(1)	0.61(3)[a]
	296	0.58(1)	0.0153(3)	0.60(1)	0.60(6)[b]
	311	0.63(1)	0.0165(3)	0.64(1)	0.62(4)[a]
	600	1.62(3)	0.045(2)	1.64(3)	1.56(6)[b]
	795	2.48(4)	0.071(2)	2.49(4)	2.39(6)[b]
	995	3.48(5)	0.097(2)	3.48(5)	3.48(11)[b]
3	296	0.352(6)	0.0194(3)	0.370(6)	0.39(1)[b]
	600	1.06(2)	0.048(2)	1.10(2)	1.10(5)[b]
	795	1.67(3)	0.071(2)	1.71(3)	1.82(11)[b]
	995	2.40(4)	0.112(2)	2.44(4)	2.54(5)[b]
4	296	0.221(4)	0.0274(4)	0.247(4)	0.31(5)[b]
	600	0.69(2)	0.061(2)	0.74(1)	0.81(5)[b]
	795	1.10(2)	0.085(2)	1.17(2)	1.31(8)[b]
	995	1.62(3)	0.112(2)	1.70(3)	1.86(4)[b]

[a]Experimental values from Ref. [22].

[b]Experimental values from Ref. [23].

Table 2: Pressure shift coefficients of the $S_0(j)$ lines in 10^{-3} cm^{-1} amg^{-1}. Besides the typical Lorentzian contribution, δ_0, we present the effective shift of the spectral line, $\delta^\dagger$, taking into account all the line-shape effects (both the velocity-changing collisions and speed-dependent effects). The values in parenthesis indicate the 1σ standard uncertainty.

j	Temperature (K)	δ_0	$\delta^\dagger$	Experiment
0	23.3	-0.063(2)	-0.063(2)	-0.07(13)[a]
	45	0.0107(3)	0.0105(2)	-0.01(10)[a]
	81.5	0.138(3)	0.137(2)	0.11(10)[a]
	119	0.284(4)	0.282(4)	0.35(8)[a]
	199	0.64(1)	0.64(1)	0.51(8)[a]
	292	1.10(2)	1.08(2)	1.01(10)[a]
	296	1.12(2)	1.10(2)	1.07(3)[b]
	600	2.54(4)	2.43(4)	2.30(24)[b]
	795	3.30(6)	3.09(5)	3.03(30)[b]
	995	3.94(6)	3.65(6)	3.58(35)[b]
1	23.3	-0.050(2)	-0.050(10)	-0.02(15)[a]
	45	0.082(2)	0.082(2)	0.04(13)[a]
	81.5	0.285(5)	0.284(6)	0.29(8)[a]
	119	0.48(1)	0.48(1)	0.47(10)[a]
	199	0.90(2)	0.89(2)	0.89(10)[a]
	292	1.37(3)	1.35(2)	1.40(10)[a]
	296	1.39(3)	1.37(2)	1.30(8)[b]
	600	2.88(5)	2.80(4)	2.65(10)[b]
	795	3.74(6)	3.59(6)	3.45(15)[b]
	995	4.54(7)	4.31(7)	3.95(19)[b]
2	199	0.87(2)	0.86(2)	0.84(10)[a]
	296	1.35(2)	1.34(2)	1.32(4)[b]
	600	2.79(4)	2.73(4)	2.66(8)[b]
	795	3.65(6)	3.55(6)	3.40(8)[b]
	995	4.49(7)	4.32(7)	3.95(7)[b]
3	296	1.53(3)	1.52(3)	1.50(5)[b]
	600	3.00(4)	2.96(5)	2.79(13)[b]
	795	3.87(6)	3.79(6)	3.65(5)[b]
	995	4.71(7)	4.59(7)	4.24(11)[b]
4	296	1.84(3)	1.83(3)	1.51(9)[b]
	600	3.48(6)	3.45(5)	3.33(6)[b]
	795	4.41(7)	4.35(7)	4.21(16)[b]
	995	5.29(8)	5.20(8)	4.96(12)[b]

[a]Experimental values from Ref. [22].

[b]Experimental values from Ref. [23].

4.3. Comparison with the experimental data

We compared the values of the pressure broadening and shift coefficients presented here with the available experimental data for $S_0(j = 0 - 4)$ lines, reported by Hermans et al. [22] and Michaut et al. [23]. The data are gathered in the Tables 1 and 2. Due to the fact that some of the experimental data were reported for temperatures outside of our grid, we performed additional calculations for them.

Overall, the agreement between our calculations and the experimental results is quite well. For the pressure broadening coefficient, a slight disagreement between theory and experiment can be observed in two cases: for temperatures below 50 K and for temperatures above 600 K. The disagreement in the low-temperature range was already reported in Ref. [1], for the $S_0(1)$ line and we still have no explanation for that. In the high-temperature case, the discrepancy is reduced if the contributions from the inhomogeneous broadening due to the speed dependence of the collisional shift and narrowing due to the speed dependence of the collisional broadening [24] are taken into account (see Tables 1, 3 and 5 of Ref. [1]). The values of the line broadening and shift corrected for these line-shape effects, $\gamma^\dagger$ and $\delta^\dagger$, are shown in Tables 1 and 2. The detailed discussion on how to calculate the speed dependence of collisional broadening and shift from the generalized spectroscopic cross section is given in Ref. [25], see Eq. (23) therein. Apart from the temperatures below 50 K, the largest disagreement between $\gamma^\dagger$ and the experimental results is 1.8σ combined standard uncertainty.

In case of the pressure shift coefficient, for low temperatures the uncertainty of the experimental data is quite large, and our results lie within the error bars. For larger temperatures we observe a slight disagreement with the experimental data, that was also noticed for the $S_0(1)$ line in Ref. [1]. The shift calculated after taking into account the speed-dependent effects has reduced this disagreement, and the largest discrepancy is 2.3σ.

In Ref. [23] the authors state that the inhomogeneous broadening could be neglected for the S_0 lines in the He-perturbed H_2. The results, presented

in Table 1 contradict this statement. In order to more explicitly present the influence of the inhomogeneous broadening and the speed dependence of the line-shape parameters, let us recall that if the speed dependence is approximated by the simple quadratic function and the velocity-changing collisions by the hard-collisions model, then the above mentioned inhomogeneous broadening is [26]:

$$\gamma_\delta = \frac{3}{2}\frac{\delta_2^2}{\tilde{\nu}_{opt}^r}, \tag{9}$$

where δ_2 is a parameter quantifying the magnitude of the speed dependence of the collisional shift within the quadratic approximation. Equation (9) is true for $\tilde{\nu}_{opt}^r \gg \delta_2$, which is well obeyed for molecular hydrogen. Additionally, if this condition is satisfied, the shape of the inhomogeneous component is Lorentzian, and can be simply added to γ_0. We present the values of γ_δ in Table 1. If there would not be any narrowing due to the speed dependence of the pressure broadening coefficient then the difference between $\gamma^\dagger$ and γ_0 would exactly match γ_δ. For some lines this difference is almost as large as γ_δ (for instance for the $S_0(4)$ line at 995 K), which means that the speed dependence of the collisional shift is considerably larger than the speed dependence of the collisional broadening (which is not explicitly presented here). For other cases, the speed dependence of the broadening dominates, effectively resulting in narrowing of the spectral line, and thus $\gamma^\dagger < \gamma_0$.

5. Accuracy of the calculations

The close-coupling scheme is the most accurate method of obtaining the line-shape parameters. However, there are several factors that could influence the accuracy of the results presented in this paper. The most important one is the accuracy of the potential energy surface used in the calculations. We made use of the most accurate PES available for the H_2-He system [4], which is an extension of the previous one [7]. Very conservative estimations of the accuracy of the used PES indicate the uncertainties of the interaction energies, for instance, near the minimum are not larger than 1%. We repeated calculations

for the $S_0(1)$ and $S_1(1)$ lines to check how such slight change of the isotropic radial terms $V_{\lambda=0,v,j,v',j'}$ (R) (multiplication by 1.01) could influence the final line-shape parameters. For the purely rotational line, for temperatures above 50 K, the relative differences between the parameters obtained with modified and correct radial terms were below 0.4%. For the remaining temperatures (5, 10, 25 and 50 K), the differences were 2%. For the $S_1(1)$ line, the relative differences were below 1% for all temperatures. However, as stated previously, the estimates of the uncertainty of the PES were quite conservative.

Other factors that could influence the accuracy of the calculations come from the numerical methods of solving the close-coupling equations. Let us remind that we used MOLSCAT code for that purpose [6]. Firstly, there are several parameters of the used propagator that could slightly modify the output of the program. We made use of the hybrid modified log-derivative Airy propagator of Manolopoulos and Alexander (setting INTFLG=8 in the MOLSCAT code), which uses the diabatic modified log-derivative method for intermolecular distances R between RMIN and RMID, and the Airy propagator between RMID and RMAX (when the propagator reaches R = RMAX, the calculations are terminated), where RMIN, RMID and RMAX are parameters that are set manually. In all calculations the values of these three parameters where set to 1 a_0, 20 a_0 and 100 a_0, respectively. The change of the RMAX parameter could potentially influence the values of the cross sections for small kinetic energies, as the long range interactions are mostly important in that region (see Sec. 4.1 or Appendix C of Ref. [4]). However, increasing this parameter to 200 a_0 has rather small influence on the output cross sections in that case, and the line-shape parameters for the $S_0(1)$ and $S_1(1)$ lines obtained this way differ from the ones reported in this work only by less than 0.02%. Thus, we can safely state that the error coming from this parameter is negligible.

The start point of the propagation, controlled by RMIN, should be placed deep in the potential wall, and the value of 1 a_0 satisfies this condition. Additional tests were performed for several kinetic energies for the $S_1(1)$ line, to determine if increasing the range of the propagation (by setting RMIN = 0.5 a_0)

could influence the outcoming results. No significant difference was observed for any of the final line-shape parameters. Thus we believe that there is no significant error coming from this parameter. Note that MOLSCAT allows RMIN and RMAX not to be fixed but to be determined internally for each new total angular momentum. No significant changes were obtained.

Another factor influencing the results comes from the step size of the chosen propagator, which, in the MOLSCAT code, can be controlled by variables STEP or DR. STEPS is the number of steps per half-wavelength for the open channel of the highest kinetic energy in the asymptotic region [6]. Through the DR variable the user can declare the initial step size explicitly. A wrong step could strongly modify the results, especially for kinetic energies below 1 cm^{-1}. We note here that both pressure shifting cross section and imaginary part of the Dicke cross section are very sensitive to the changes of these parameters. We performed tests using different step sizes for several lines from 0-5 band and we could determine the error associated with this factor: 0.5% for the pressure broadening coefficient and the real part of the Dicke parameter and 1% for the pressure shift coefficient and the imaginary part of the Dicke parameter.

The number of closed levels used in the calculations could also contribute to the uncertainty of the results. For all investigated lines we kept one closed level, but we made additional calculations with two closed levels to check how this could influence the final line-shape parameters. The relative differences between these results where about 0.5%. Moreover, we checked how truncating the basis in the calculations for highest kinetic energies (above 8000 cm^{-1}) could modify the results. We found that such truncation could influence the line-shape parameters only for T = 2000 K. This error is 0.5% large.

Taking into consideration the most significant factors: the accuracy of the PES, the error coming from the step size of the propagator and from the number of closed levels, we can conservatively estimate the accuracy of the line-shape parameters presented here. The uncertainties for temperatures above 50 K and below 2000 K are 2.5% large. We stress here, that the accuracy of the calculations deteriorates at 2000 K, due to the fact, that the Maxwell-Boltzmann

distribution at this temperature is still significant for kinetic energies about 9000 cm^{-1}, and calculations should be performed for even larger kinetic energies. Therefore, we estimate that the uncertainty for T = 2000 K is 3% large. For temperatures below 50 K, the uncertainties of the line-shape parameters are 3.5% large. All the error bars reported in this work are 1σ standard uncertainties.

6. Conclusion

We provided a set of line-shape parameters for S and O branches of H_2 in He for 18 temperatures between 5 and 2000 K. We investigated 60 transitions in total, for vibrational bands ranging from 0-0 up to 0-5 and for rotational levels from j=0 to j=5 for S lines, and from j=2 to j=5 for O lines. We used the most accurate available PES for this system [4] and performed close-coupling calculations using the MOLSCAT code [6]. The generalized spectroscopic cross sections were obtained from the S-matrix elements, for kinetic energies ranging from 0.1 up to 9000 cm^{-1}. The final line-shape parameters reported here are the standard pressure broadening and shifting coefficients and the real and imaginary parts of Dicke parameters. All these quantities, along with the generalized cross sections, can be found in the supplementary materials [20]. The results of this investigation provide a reference data for astrophysical and planetary studies. The present work completes the previously reported calculations on the Q-branches [4] and together with Ref. [4] provide data that will be used in our forthcoming article [27] to generate the first comprehensive dataset of line-shape parameters for the HITRAN database [28].

7. Acknowledgement

The research is supported by the National Science Centre, Poland, Project No. 2015/19/D/ST2/02195. The research is part of the program of the National Laboratory FAMO in Toruń, Poland.

References

References

[1] F. Thibault, P. Wcisło, R. Ciuryło, A test of H_2-He potential energy surfaces, EPJD 70 (2016) 236. doi:10.1140/epjd/e2016-70114-9.

[2] K. H. Baines, M. E. Mickelson, L. E. Larson, D. W. Ferguson, The abundances of methane and ortho/para hydrogen on Uranus and Neptune: Implications of new laboratory 4-0 H_2 quadrupole line parameters, Icarus 114 (1995) 328. doi:10.1006/icar.1995.1065.

[3] W. M. Hayden Smith, C. P. Conner, J. Simon, W. V. Schempp, W. Macy, The H_2 4-0 S(0,1, and 2) quadrupole features in Jupiter, Icarus 81 (1989) 429. doi:10.1016/0019-1035(89)90062-6.

[4] F. Thibault, K. Patkowski, P. Zuchowski, H. Jóźwiak, P. Wcisło, R. Ciuryło, Rovibrational line-shape parameters for H_2 in He and new H_2-He potential energy surface, J Quant Spectrosc Radiat Transfer 202 (2017) 308. doi:10.1016/j.jqsrt.2017.08.014.

[5] R. Z. Martinez, D. Bermejo, F. Thibault, P. Wcisło, Testing the ab initio quantum-scattering calculations for the D_2-He benchmark system with stimulated Raman spectroscopy, J Raman Spectrosc 49 (2018) 1339. doi:10.1002/jrs.5391.

[6] J. M. Hutson, S. Green, Molscat version14, Collaborative Computational Project 6 of the UK Science and Engineering Research Council, Daresbury Laboratory, UK, 1995.

[7] B. W. Bakr, D. G. A. Smith, K. Patkowski, Highly accurate potential energy surface for the He-H_2 dimer, J Chem Phys 139 (2013) 144305. doi:10.1063/1.4824299.

[8] J. Schaefer, W. E. Köhler, Quantum calculations of rotational and NMR relaxation, depolarized Rayleigh and rotational Raman line shapes

for H_2(HD)He mixtures, Physica A 129 (1985) 469. doi:10.1016/0378-4371(85)90181-5.

[9] P. Muchnick, A. Russek, The HeH_2 energy surface, J Chem Phys 100 (1994) 4336. doi:10.1063/1.466316.

[10] A. I. Boothroyd, P. G. Martin, M. Peterson, Accurate analytic HeH_2 potential energy surface from a greatly expanded set of ab initio energies, J Chem Phys 119 (2003) 3187. doi:10.1063/1.1589734.

[11] R. Shafer, R. G. Gordon, Quantum scattering theory of rotational relaxation and spectral line shapes in H_2 - He gas mixtures, J Chem Phys 58 (1973) 5422. doi:10.1063/1.1679162.

[12] M. L. Dubernet, P. A. Tuckey, Raman Q and S line broadening and shifting coefficients: some commonly used assumptions revisited, Chem Phys Lett 300 (1999) 275. doi:10.1016/S0009-2614(98)01334-7.

[13] L. Monchick, L. Hunter, Diatomic-diatomic molecular collision integrals for pressure broadening and dicke narrowing: a generalization of Hess ´ s theory., J Chem Phys 85 (1986) 713. doi:10.1063/1.451277.

[14] J. Schaefer, L. Monchick, Line broadening of HD immersed in He and H_2 gas., Astron Astrophys 859 (1992) 265. doi:10.1063/1.453612.

[15] A. P. Yutsis, I. B. Levinson, V. V. Vangas, Theory of angular momentum, Israel Program for Scientific Translations, Jerusalem, 1962.

[16] A. Ben-Reuven, Symmetry considerations in pressure-broadening theory, Phys Rev 141 (1966) 34. doi:10.1103/PhysRev.141.34.

[17] A. Ben-Reuven, Impact broadening of microwave spectra, Phys Rev 145 (1966) 7. doi:10.1103/PhysRev.145.7.

[18] G. C. Corey, F. R. McCourt, Dicke narrowing and collisional broadening of spectral lines in dilute molecular gases,, J Chem Phys 81 (1984) 2318. doi:10.1063/1.447930.

[19] J.Komasa, K. Piszczatowski, G. Lach, M. Przybytek, B. Jeziorski, K. Pachucki, Quantum electrodynamics effects in rovibrational spectra of molecular Hydrogen, J Chem Theory Comput 7 (2011) 3105. doi:10.1021/ct200438t.

[20] H. Jóźwiak, F. Thibault, N. Stolarczyk, P. Wcisło, Supplementary material for PB-, PS- and Dicke coefficients, J Quant Spectrosc Radiat Transfer.

[21] J. W. Forsman, J. Bonamy, D. Robert, J. P. Berger, R. Saint-Loup, H. Berger, H_2-He vibrational line-shape parameters: Measurement and semiclassical calculation, Phys Rev A 52 (1995) 2652. doi:10.1103/PhysRevA.52.2652.

[22] P. W. Hermans, A. V. Die, H. F. P. Knaap, J. J. M. Beenakker, Measurements on the influence of binary collisions on the depolarized Rayleigh and rotational Raman lines for H_2-noble gas systems at low temperatures, Physica A 132 (1985) 233. doi:10.1016/0378-4371(85)90010-X.

[23] X. Michaut, R. Saint-Loup, H. Berger, M. Dubernet, P. Joubert, J. Bonamy, Investigations of pure rotational transitions of H_2 self-perturbed and perturbed by He. I. Measurement, modeling, and quantum calculations, J Chem Phys 109 (1998) 951. doi:10.1063/1.476638.

[24] P. Wcisło, F. Thibault, H. Cybulski, R. Ciuryło, Strong competition between velocity-changing and phase- or state-changing collisions in H_2 spectra perturbed by Ar, Phys Rev A 91 (2015) 052505. doi:10.1103/PhysRevA.91.052505.

[25] P. Wcisło, F. Thibault, M. Zaborowski, S. Wójtewicz, A. Cygan, G. Kowzan, P. Masłowski, J. Komasa, M. Puchalski, K. Pachucki, R. Ciuryło, D. Lisak, Accurate deuterium spectroscopy for fundamental studies, J Quant Spectrosc Radiat Transfer 213 (2018) 41. doi:10.1016/j.jqsrt.2018.04.011.

[26] P. Wcisło, I. Gordon, H. Tran, Y. Tan, S.-M. Hu, A. Campargue, S. Kassi, D. Romanini, C. Hill, R. Kochanov, L. Rothman, The implementation of non-voigt line profiles in the hitran database: H2 case study, J Quant Spectrosc Radiat Transfer 177 (2016) 75. doi:https://doi.org/10.1016/j.jqsrt.2016.01.024.

[27] P. Wcisło, F. Thibault, N. Stolarczyk, H. Jóźwiak, M. Słowiński, M. Konefał, S. Kassi, A. Campargue, Y. Tan, J. Wang, A.-W. Liu, S.-M. Hu, K. Patkowski, R. Ciuryło, D. Lisak, R. Kochanov, I. Gordon, First comprehensive dataset of beyond-voigt line-shape parameters from ab initio quantum scattering calculations for the HITRAN database, in preparation.

[28] I. Gordon, L. Rothman, C. Hill, R. Kochanov, Y. Tan, P. Bernath, M. Birk, V. Boudon, A. Campargue, K. Chance, B. Drouin, J.-M. Flaud, R. Gamache, J. Hodges, D. Jacquemart, V. Perevalov, A. Perrin, K. Shine, M.-A. Smith, J. Tennyson, G. Toon, H. Tran, V. Tyuterev, A. Barbe, A. Csszr, V. Devi, T. Furtenbacher, J. Harrison, J.-M. Hartmann, A. Jolly, T. Johnson, T. Karman, I. Kleiner, A. Kyuberis, J. Loos, O. Lyulin, S. Massie, S. Mikhailenko, N. Moazzen-Ahmadi, H. Mller, O. Naumenko, A. Nikitin, O. Polyansky, M. Rey, M. Rotger, S. Sharpe, K. Sung, E. Starikova, S. Tashkun, J. V. Auwera, G. Wagner, J. Wilzewski, P. Wcisło, S. Yu, E. Zak, The HITRAN2016 molecular spectroscopic database, J Quant Spectrosc Radiat Transfer 203 (2017) 3, HITRAN2016 Special Issue. doi:https://doi.org/10.1016/j.jqsrt.2017.06.038.